Clemson University
College of Engineering and Science
Control and Robotics (CRB) Technical Report

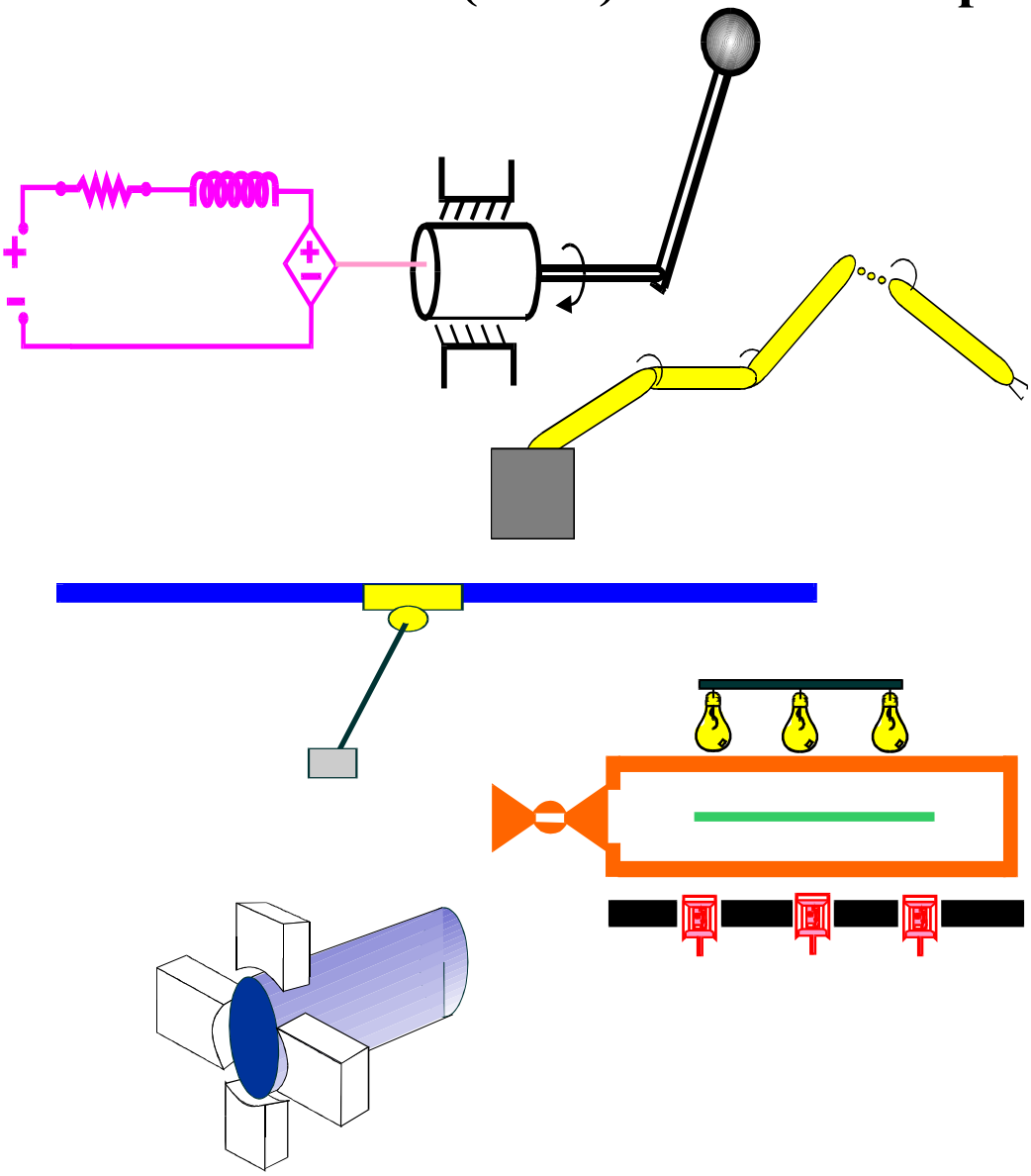

Number: CU/CRB/8/20/04/#1

Title: Adaptive Tracking Control of On-Line Path Planners: Velocity Fields and Navigation Functions

Authors: M. McIntyre, W. Dixon, D. Dawson, and B. Xian

Report Documentation Page

Form Approved
OMB No. 0704-0188

1. REPORT DATE	2. REPORT TYPE	3. DATES COVERED
2004		**00-00-2004 to 00-00-2004**

4. TITLE AND SUBTITLE	5a. CONTRACT NUMBER
Adaptive Tracking Control of On-Line Path Planners: Velocity Fields and Navigation Functions	5b. GRANT NUMBER
	5c. PROGRAM ELEMENT NUMBER
6. AUTHOR(S)	5d. PROJECT NUMBER
	5e. TASK NUMBER
	5f. WORK UNIT NUMBER
7. PERFORMING ORGANIZATION NAME(S) AND ADDRESS(ES) **Clemson University,Department of Electrical & Computer Engineering,Clemson,SC,29634-0915**	8. PERFORMING ORGANIZATION REPORT NUMBER
9. SPONSORING/MONITORING AGENCY NAME(S) AND ADDRESS(ES)	10. SPONSOR/MONITOR'S ACRONYM(S)
	11. SPONSOR/MONITOR'S REPORT NUMBER(S)

12. DISTRIBUTION/AVAILABILITY STATEMENT
Approved for public release; distribution unlimited

13. SUPPLEMENTARY NOTES
The original document contains color images.

14. ABSTRACT

15. SUBJECT TERMS

16. SECURITY CLASSIFICATION OF:			17. LIMITATION OF ABSTRACT	18. NUMBER OF PAGES	19a. NAME OF RESPONSIBLE PERSON
a. REPORT	b. ABSTRACT	c. THIS PAGE			
unclassified	**unclassified**	**unclassified**		**24**	

Adaptive Tracking Control of On-Line Path Planners: Velocity Fields and Navigation Functions*

M. L. McIntyre,† W. E. Dixon,‡ D. M. Dawson,† and B. Xian†

†Department of Electrical & Computer Engineering, Clemson University, Clemson, SC 29634-0915

‡Department of Mechanical & Aerospace Engineering, University of Florida, Gainesville, FL 32611-6250

E-mail: wdixon@ufl.edu

Abstract: Traditionally, robot control research has focused on the position tracking problem where the objective is to force the robot's end-effector to follow an a priori known desired time dependent trajectory. Motivated by task objectives that are more effectively described by on-line, state-dependent trajectories, two adaptive tracking controllers are developed in this paper that accommodate on-line path planning objectives. An example adaptive controller is first modified to achieve velocity field tracking in the presence of parametric uncertainty in the robot dynamics. The development aims to relax the typical assumption that the integral of the velocity field is bounded by incorporating a norm squared gradient term in the control design so that the boundedness of all signals can be proven. An extension is then provided that targets the trajectory planning problem where the task objective can be described as the desire to move to a goal configuration while avoiding known obstacles. Specifically, an adaptive navigation function based controller is designed to provide a path from an initial condition inside the free configuration space of the robot manipulator to the goal configuration. Experimental results for each controller are provided to illustrate proof of validation of the approaches.

1 Introduction

Traditionally, robot control researchers have focused on the position tracking problem where the objective is to force the robot to follow a desired time dependent trajectory. Since the objective is encoded in terms of a time dependent trajectory, the robot may be forced to follow an unknown course to catch up with the desired trajectory in the presence of a large initial error. For example, several researchers have reported the so called radial reduction phenomena (e.g., [20], [21]) in which the actual path followed has a smaller radius than the specified trajectory. In light of this phenomena, the control objective for many robotic tasks are more appropriately encoded as a contour following problem in which the objective is to force the robot to follow a state-dependent function that describes the contour. One example of a control strategy aimed at the contour following problem is velocity field control (VFC) where the desired contour is describe by a velocity tangent vector [22]. The advantages of the VFC approach can be summarized as follows.[1]

*This research was supported in part by U.S. NSF Grant DMI-9457967, ONR Grant N00014-99-1-0589, a DOC Grant, an ARO Automotive Center Grant, and in part by the Defence Advanced Research Project Agency (DARPA) through the Space Naval Warfare System Center, San Diego, contract N66001-03-R-8043.

[1]See [4], [20], and [22] for a more thorough discussion of the advantages and differences of VFC with respect to traditional trajectory tracking control.

- The velocity field error more effectively penalizes the robot for leaving the desired contour.
- The control task can be specified invariant of the task execution speed.
- Task coordination and synchronization is more explicit for contour following.

The ability for a velocity field to encode certain contour following tasks has recently prompted researchers to investigate VFC for various applications. For example, Li and Horowitz utilized a passive VFC approach to control robot manipulators for contour following applications in [22], and more recently, Dee and Li used VFC to achieve passive bilateral teleoperation of robot manipulators in [18]. The authors of [20] utilized a passive VFC approach to develop a force controller for robot manipulator contour following applications. Other relevant work utilizing VFC approaches are given in the following: [21] and [23]. Yamakita et al. investigated the application of passive VFC to cooperative mobile robots and cooperative robot manipulators in [33] and [34], respectively. Typically, VFC is based on a nonlinear control approach where exact model knowledge of the system dynamics are required. Motivated by the desire to account for uncertainty in the robot dynamics, Cervantes et al. developed a robust VFC in [4]. Specifically, in [4] a proportional-integral controller was developed that achieved semiglobal practical stabilization of the velocity field tracking errors despite uncertainty in the robot dynamics. From a review of VFC literature, it can also be determined that previous research efforts have focused on ensuring the robot tracks the velocity field, but no development has been provided to ensure the link position remains bounded. The result in [4] acknowledged the issue of boundedness of the robot position; however, the issue is simply addressed by an assumption that the following norm

$$\left\| q(0) + \int_0^t \vartheta(q(\sigma))d\sigma \right\| \tag{1}$$

yields globally bounded trajectories, where $q(t)$ denotes the position, and $\vartheta(\cdot)$ denotes the velocity field.

In addition to VFC, some task objectives are motivated by the need to follow a trajectory to a desired goal configuration while avoiding known obstacles in the configuration space. For this class of problems, it is more important for the robot to follow an obstacle free path to the desired goal point than it is to meet a time-based requirement. Numerous researchers have investigated algorithms to address this motion control problem. A comprehensive summary of techniques that address the classic geometric problem of constructing a collision-free path and traditional path planning algorithms is provided in Section 9, "Literature Landmarks", of Chapter 1 of [16]. Since the pioneering work by Khatib in [11], it is clear that the construction and use of potential functions has continued to be one of the mainstream approaches to robotic task execution among known obstacles. In short, potential functions produce a repulsive potential field around the boundary of the robot task-space and obstacles and an attractive potential field at the goal configuration. A comprehensive overview of research directed at potential functions is provided in [16]. One criticism of the potential function approach is that local minima can occur that can cause the robot to "get stuck" without reaching the goal position. Several researchers have proposed approaches to address the local minima issue (e.g., see [1], [2], [5], [12], [32]). One approach to address the local minima issue was provided by Koditschek in [13] for holonomic systems (see also [14] and [27]) that is based on a special kind of potential function, coined a navigation function, that has a refined mathematical structure which guarantees a unique minimum exists. By leveraging from previous results directed at classic (holonomic) systems, more recent research has focused on the development of potential

function-based approaches for nonholonomic systems. For a review of this literature see [3], [7], [8], [9], [15], [17], [23], [25], [27], [30], and [31].

The aim of this paper is to illustrate how an example adaptive controller (e.g., the benchmark adaptive tracking controller presented in [28]) can be modified to incorporate trajectory planning techniques with the controller. To this end, two adaptive controllers are developed. The first controller focuses on the VFC problem. Specifically, the benchmark adaptive controller given in [28] is modified to yield VFC in the presence of parametric uncertainty. The contribution of the development is that velocity field tracking is achieved by incorporating a norm squared gradient term in the control design that is used to prove the link positions are bounded through a Lyapunov-analysis rather than by an assumption. In lieu of the assumption in (1), the VFC development is based on the selection of a velocity field that is first order differentiable, and that a first order differentiable, nonnegative function $V(q) \in \mathbb{R}$ exists such that the following inequality holds

$$\frac{\partial V(q)}{\partial q}\vartheta(q) \leq -\gamma_3(\|q\|) + \zeta_0 \tag{2}$$

where $\frac{\partial V(q)}{\partial q}$ denotes the partial derivative of $V(q)$ with respect to $q(t)$, $\gamma_3(\cdot) \in \mathbb{R}$ is a class $\mathcal{K}$ function[2], and $\zeta_0 \in \mathbb{R}$ is a nonnegative constant. That is, in lieu of the assumption in (1) this paper introduces a stability-based condition on the velocity field. It is interesting to note that the velocity field described in the experimental results provided in [4] can be shown to satisfy the stability-based condition in (2) *(see Appendix A for proof)*. As an extension to the VFC problem, a navigation function is incorporated with the benchmark adaptive controller in [28] to track a reference trajectory that yields a collision free path to a constant goal point in an obstacle cluttered environment with known obstacles.

This paper is organized as follows. In Section 2, the dynamic model for a robot manipulator is provided. In Section 3, the VFC development is presented, including a two-part stability analysis. The first analysis proves that if a velocity field tracking signal is square integrable then the link position is globally uniformly bounded (GUB). The second analysis proves that the velocity field tracking signal is square integrable, all the system states are bounded, and that the velocity field tracking error converges to zero despite parametric uncertainty in the dynamic model. Experimental results based on the velocity field presented in [4] are provided to demonstrate proof of validation of the VFC approach. In Section 4, a navigation function based trajectory planning and control development is presented, along with the stability analysis. This analysis proves that a backstepping signal is square integrable, all the system states are bounded, and that the robot manipulator will track an obstacle free path to a goal point, despite parametric uncertainty in the dynamic model. Experimental results for the adaptive navigation function controller is provided to demonstrate proof of validation of the approach. Concluding remarks are provided in Section 5.

2 System Model

The mathematical model for an n-DOF robotic manipulator is assumed to have the following form

$$M(q)\ddot{q} + V_m(q,\dot{q})\dot{q} + G(q) = \tau. \tag{3}$$

In (3), $q(t)$, $\dot{q}(t)$, $\ddot{q}(t) \in \mathbb{R}^n$ denote the link position, velocity, and acceleration, respectively, $M(q) \in \mathbb{R}^{n\times n}$ represents the positive-definite, symmetric inertia matrix, $V_m(q,\dot{q}) \in \mathbb{R}^{n\times n}$ represents the

[2] A continuous function $\alpha : [0,\alpha) \to [0,\infty)$ is said to belong to class $\mathcal{K}$ if it is strictly increasing and $\alpha(0) = 0$ [10].

centripetal-Coriolis terms, $G(q) \in \mathbb{R}^n$ represents the known gravitational vector, and $\tau(t) \in \mathbb{R}^n$ represents the torque input vector. The system states, $q(t)$ and $\dot{q}(t)$ are assumed to be measurable. It is also assumed that $M(q)$, $V_m(q, \dot{q})$, and $G(q) \in \mathcal{L}_\infty$ provided $q(t)$, $\dot{q}(t) \in \mathcal{L}_\infty$. The dynamic model in (3), exhibits the following properties that are utilized in the subsequent control development and stability analysis.

Property 1: The inertia matrix can be upper and lower bounded by the following inequalities [19]

$$m_1 \|\xi\|^2 \leq \xi^T M(q) \xi \leq m_2(q) \|\xi\|^2 \quad \forall \xi \in \mathbb{R}^n \tag{4}$$

where m_1 is a positive constant, $m_2(\cdot)$ is a positive function, and $\|\cdot\|$ denotes the Euclidean norm.

Property 2: The inertia and the centripetal-Coriolis matrices satisfy the following relationship [19]

$$\xi^T \left(\frac{1}{2} \dot{M}(q) - V_m(q, \dot{q}) \right) \xi = 0 \quad \forall \xi \in \mathbb{R}^n \tag{5}$$

where $\dot{M}(q)$ represents the time derivative of the inertia matrix.

Property 3: The robot dynamics given in (3) can be linearly parameterized as follows [19]

$$Y(q, \dot{q}, \ddot{q}) \theta \triangleq M(q) \ddot{q} + V_m(q, \dot{q}) \dot{q} + G(q) \tag{6}$$

where $\theta \in \mathbb{R}^p$ contains constant system parameters, and $Y(q, \dot{q}, \ddot{q}) \in \mathbb{R}^{n \times p}$ denotes a regression matrix composed of $q(t)$, $\dot{q}(t)$, and $\ddot{q}(t)$.

3 Adaptive VFC

3.1 Control Objective

As described previously, many robotic tasks can be effectively encapsulated as a velocity field. That is, the velocity field control objective can be described as commanding the robot manipulator to track a velocity field that is defined as a function of the current link position. To quantify this objective, a velocity field tracking error, denoted by $\eta_1(t) \in \mathbb{R}^n$, is defined as follows

$$\eta_1(t) \triangleq \dot{q}(t) - \vartheta(q) \tag{7}$$

where $\vartheta(\cdot) \in \mathbb{R}^n$ denotes the velocity field. To achieve the control objective, the subsequent development is based on the assumption that $q(t)$ and $\dot{q}(t)$ are measurable, and that $\vartheta(q)$ and its partial derivative $\frac{\partial \vartheta(q)}{\partial q} \in \mathbb{R}^n$, are assumed to be bounded provided $q(t) \in \mathcal{L}_\infty$.

3.2 Benchmark Control Modification

To develop the open-loop error dynamics for $\eta_1(t)$, we take the time derivative of (7) and premultiply the resulting expression by the inertia matrix as follows

$$\begin{aligned} M(q) \dot{\eta}_1 \quad = \quad & -V_m(q, \dot{q}) \dot{q} - G(q) + \tau + V_m(q, \dot{q}) \vartheta(q) \\ & - V_m(q, \dot{q}) \vartheta(q) - M(q) \frac{\partial \vartheta(q)}{\partial q} \dot{q} \end{aligned} \tag{8}$$

where (3) was utilized. From (7), the expression in (8) can be rewritten as follows

$$M(q)\dot{\eta}_1 = -V_m(q,\dot{q})\eta_1 - Y_1(q,\dot{q})\theta + \tau \tag{9}$$

where θ was introduced in (6) and $Y_1(q,\dot{q}) \in \mathbb{R}^{n\times p}$ denotes a measurable regression matrix that is defined as follows

$$Y_1(q,\dot{q})\theta \triangleq M(q)\frac{\partial \vartheta(q)}{\partial q}\dot{q} + V_m(q,\dot{q})\vartheta(q) + G(q). \tag{10}$$

Based on the open-loop error system in (9), a number of control designs could be utilized to ensure velocity field tracking (i.e., $\|\eta_1(t)\| \to 0$) given the assumption in (1). Motivated by the desire to eliminate the assumption in (1), a norm squared gradient term is incorporated in an adaptive controller introduced in [28] as follows

$$\tau(t) \triangleq -\left(K + \left\|\frac{\partial V(q)}{\partial q}\right\|^2 I_n\right)\eta_1 + Y_1(q,\dot{q})\hat{\theta}_1 \tag{11}$$

where $K \in \mathbb{R}^{n\times n}$ is a constant, positive definite diagonal matrix, $I_n \in \mathbb{R}^{n\times n}$ is the standard $n \times n$ identity matrix, and $\frac{\partial V(q)}{\partial q}$ was introduced in (2). In (11), $\hat{\theta}_1(t) \in \mathbb{R}^p$ denotes a parameter estimate that is generated by the following gradient update law

$$\dot{\hat{\theta}}_1(t) = -\Gamma_1 Y_1^T(q,\dot{q})\eta_1 \tag{12}$$

where $\Gamma_1 \in \mathbb{R}^{p\times p}$ is a constant, positive definite diagonal matrix. After substituting (11) into (9), the following closed-loop error system can be obtained

$$M(q)\dot{\eta}_1 = -V_m(q,\dot{q})\eta_1 - Y_1(q,\dot{q})\tilde{\theta}_1 - \left(K + \left\|\frac{\partial V(q)}{\partial q}\right\|^2 I_n\right)\eta_1 \tag{13}$$

where the parameter estimation error signal $\tilde{\theta}_1(t) \in \mathbb{R}^p$ is defined as follows

$$\tilde{\theta}_1(t) \triangleq \theta - \hat{\theta}_1. \tag{14}$$

Remark 1 *It is required for the selection of a particular $\vartheta(q)$ and $V(q)$, that the inequality as defined in (2) must hold. In the event that this condition does not hold, the tracking objective is not guaranteed as described by the subsequent stability analysis.*

Remark 2 *While the control development is based on a modification of the adaptive controller introduced in [28], the norm squared gradient term could also be incorporated in other benchmark controllers to yield similar results (e.g., sliding mode controllers).*

3.3 Stability Analysis

To facilitate the subsequent stability analysis, the following preliminary theorem is utilized.

Theorem 1 *Let $\bar{V}(t) \in \mathbb{R}$ denote the following nonnegative, continuous differentiable function*

$$\bar{V}(t) \triangleq V(q) + P(t)$$

where $V(q) \in \mathbb{R}$ denotes a nonnegative, continuous differentiable function that satisfies (2) and the following inequalities

$$0 \leq \gamma_1(\|q\|) \leq V(q) \leq \gamma_2(\|q\|)$$

where $\gamma_1(\cdot)$, $\gamma_2(\cdot)$ are class $\mathcal{K}$ functions, and $P(t) \in \mathbb{R}$ denotes the following nonnegative, continuous differentiable function

$$P(t) \triangleq \gamma - \int_{t_0}^{t} \varepsilon^2(\sigma) d\sigma \tag{15}$$

where $\gamma \in \mathbb{R}$ is a positive constant, and $\varepsilon(t) \in \mathbb{R}$ is defined as follows

$$\varepsilon \triangleq \left\| \frac{\partial V(q)}{\partial q} \right\| \|\eta_1\|. \tag{16}$$

If $\varepsilon(t)$ is a square integrable function, where

$$\int_{t_0}^{t} \varepsilon^2(\sigma) d\sigma \leq \gamma,$$

and if after utilizing (7), the time derivative of $\bar{V}(t)$ satisfies the following inequality

$$\dot{\bar{V}}(t) \leq -\gamma_3(\|q\|) + \xi_0 \tag{17}$$

where $\gamma_3(q)$ is the class $\mathcal{K}$ function introduced in (2), and $\xi_0 \in \mathbb{R}$ denotes a positive constant, then $q(t)$ is global uniformly bounded.

Proof: The time derivative of $\bar{V}(t)$ can be expressed as follows

$$\dot{\bar{V}}(t) = \frac{\partial V(q)}{\partial q} \vartheta(q) + \frac{\partial V(q)}{\partial q} \eta_1 - \varepsilon^2(t)$$

where (7) and (15) were utilized. By exploiting the inequality introduced in (2) and the definition for $\varepsilon(t)$ provided in (16), the following inequality can be obtained

$$\dot{\bar{V}}(t) \leq -\gamma_3(\|q\|) + \zeta_0 + \left[\varepsilon(t) - \varepsilon^2(t)\right]. \tag{18}$$

After completing the squares on the bracketed terms in (18), the inequality introduced in (17) is obtained where

$$\xi_0 \triangleq \zeta_0 + \frac{1}{4}.$$

Hence, if $\varepsilon(t) \in \mathcal{L}_2$, then Lemma 1 in Appendix B can be used to prove that $q(t)$ is GUB. ■

In the following analysis, we first prove that $\varepsilon(t) \in \mathcal{L}_2$. Based on the conclusion that $\varepsilon(t) \in \mathcal{L}_2$, the result from Theorem 1 is utilized to ensure that $q(t)$ is bounded under the proposed adaptive controller given in (11) and (12).

Theorem 2 *The adaptive VFC given in (11) and (12) yields global velocity field tracking in the sense that*

$$\|\eta_1(t)\| \to 0 \quad as \quad t \to \infty. \tag{19}$$

Proof: Let $V_1(t) \in \mathbb{R}$ denote the following nonnegative function

$$V_1 \triangleq \frac{1}{2}\eta_1^T M \eta_1 + \frac{1}{2}\tilde{\theta}_1^T \Gamma_1^{-1} \tilde{\theta}_1. \tag{20}$$

After taking the time derivative of (20) the following expression can be obtained

$$\dot{V}_1 = -\eta_1^T \left(Y_1(q, \dot{q})\tilde{\theta}_1 + \left(K + \left\| \frac{\partial V(q)}{\partial q} \right\|^2 I_n \right) \eta_1 \right) - \tilde{\theta}_1^T \Gamma_1^{-1} \dot{\hat{\theta}}_1 \tag{21}$$

where (5) and (13) were utilized. After utilizing the parameter update law given in (12), the expression given in (21) can be rewritten as follows

$$\dot{V}_1 = -\eta_1^T \left(K + \left\| \frac{\partial V(q)}{\partial q} \right\|^2 I_n \right) \eta_1. \tag{22}$$

The expressions given in (16), (20), and (22) can be used to conclude that $\eta_1(t)$, $\tilde{\theta}_1(t) \in \mathcal{L}_\infty$ and $\eta_1(t), \varepsilon(t) \in \mathcal{L}_2$. Based on the fact that $\varepsilon(t) \in \mathcal{L}_2$, the results from Theorem 1 can be used to prove that $q(t) \in \mathcal{L}_\infty$. Since $q(t) \in \mathcal{L}_\infty$, the assumption that $\vartheta(q)$ and$\frac{\partial \vartheta(q)}{\partial q} \in \mathcal{L}_\infty$ can be used to conclude that $\dot{q}(t) \in \mathcal{L}_\infty$, where the expression in (7) was utilized. Based on the fact that $\tilde{\theta}_1(t) \in \mathcal{L}_\infty$, the expression in (14) can be used to prove that $\hat{\theta}_1(t) \in \mathcal{L}_\infty$. Based on the facts that $M(q)$, $V_m(q, \dot{q})$, $G(q) \in \mathcal{L}_\infty$ along with the facts that $q(t)$, $\dot{q}(t)$, $\vartheta(q)$, $\frac{\partial \vartheta(q)}{\partial q} \in \mathcal{L}_\infty$, and (10) can be used to prove that $Y_1(q, \dot{q}) \in \mathcal{L}_\infty$. The facts that $Y_1(q, \dot{q})$, $\hat{\theta}_1(t), \eta_1(t) \in \mathcal{L}_\infty$ and the fact that $\frac{\partial V(q)}{\partial q} \in \mathcal{L}_\infty$ (based on Theorem 1) can be used along with (11) to prove that $\tau(t) \in \mathcal{L}_\infty$. Based on the previous bounding statements, the expression given in (13) can be used to prove that $\dot{\eta}_1(t) \in \mathcal{L}_\infty$. Given that $\eta_1(t)$, $\dot{\eta}_1(t) \in \mathcal{L}_\infty$ and $\eta_1(t) \in \mathcal{L}_2$, Barbalat's Lemma [28] can now be utilized to prove (19). ■

4 Navigation Function Control Extension

4.1 Control Objective

The objective in this extension is to navigate a robot's end-effector along a collision-free path to a constant goal point, denoted by $q^* \in \mathcal{D}$, where the set $\mathcal{D}$ denotes a free configuration space that is a subset of the whole configuration space with all configurations removed that involve a collision with an obstacle, and $q^* \in \mathbb{R}^n$ denotes the constant goal point in the interior of $\mathcal{D}$. Mathematically, the primary control objective can be stated as the desire to ensure that

$$q(t) \to q^* \text{ as } t \to \infty \tag{23}$$

where the secondary control is to ensure that $q(t) \in \mathcal{D}$. To achieve these two control objectives, we define $\varphi(q) \in \mathbb{R}$ as a function $\varphi(q) : \mathcal{D} \to [0, 1]$ that is assumed to satisfy the following properties:

- P1) The function $\varphi(q)$ is first order and second order differentiable Morse function [14] (i.e., $\frac{\partial}{\partial q}\varphi(q)$and $\frac{\partial}{\partial q}\left(\frac{\partial}{\partial q}\varphi(q)\right)$ exist on $\mathcal{D}$).
- P2) The function $\varphi(q)$ obtains its maximum value on the boundary of $\mathcal{D}$.
- P3) The function $\varphi(q)$ has a unique global minimum at $q(t) = q^*$.

- P4) If $\frac{\partial}{\partial q}\varphi(q) = 0$ then $q(t) = q^*$.

Based on (23) and the above definition, an auxiliary tracking error signal, denoted by $\eta_2(t) \in \mathbb{R}^n$, can be defined as follows to quantify the control objective

$$\eta_2(t) \triangleq \dot{q}(t) + \bigtriangledown\varphi(q) \tag{24}$$

where $\bigtriangledown\varphi(q) = \frac{\partial}{\partial q}\varphi(q)$ denotes the gradient vector of $\varphi(q)$ defined as follows

$$\bigtriangledown\varphi(q) \triangleq \left[\begin{array}{cccc} \frac{\partial\varphi}{\partial q_1} & \frac{\partial\varphi}{\partial q_2} & \cdots & \frac{\partial\varphi}{\partial q_n} \end{array} \right]^T. \tag{25}$$

Remark 3 *As discussed in [27], the construction of the function $\varphi(q)$, coined a navigation function, that satisfies all of the above properties for a general obstacle avoidance problem is nontrivial. Indeed, for a typical obstacle avoidance, it does not seem possible to construct $\varphi(q)$ such that $\frac{\partial}{\partial q}\varphi(q) = 0$ only at $q(t) = q^*$. That is, as discussed in [27], the appearance of interior saddle points (i.e., unstable equilibria) seems to be unavoidable; however, these unstable equilibria may have minimal impact in practice. That is, $\varphi(q)$ can be constructed as shown in [27] such that only a "few" initial conditions will result in convergence to the unstable equilibria.*

Remark 4 *The two control developments presented in the paper appear to be mathematically similar (i.e. (7) and (24)), but the control objectives are very different. The VFC objective is to achieve robot end-effector velocity tracking with a desired trajectory generated by a velocity field, $\vartheta(q)$, hence, there is no goal point. The navigation function control development utilizes a special function $\varphi(q)$, that has specific properties such that the robot's end-effector finds a collision free path to a known goal point, q^* and stops. Each signal, $\vartheta(q)$ for the VFC development, and $\varphi(q)$ for the navigation function control development must meet a set of qualifying conditions (i.e. the inequality of (2) for the VFC and P1 - P4 for the navigation function control), but these conditions are not the same, therefore the two objectives are very different.*

4.2 Benchmark Control Modification

To develop the open-loop error dynamics for $\eta_2(t)$, we take the time derivative of (24) and premultiply the resulting expression by the inertia matrix as follows

$$M\dot{\eta}_2 = -V_m(q,\dot{q})\eta_2 + Y_2(q,\dot{q})\theta + \tau. \tag{26}$$

where (3) and (24) were utilized. In (26), the linear parameterization $Y_2(q,\dot{q})\theta$ is defined as follows

$$Y_2(q,\dot{q})\theta \triangleq M(q)f(q,\dot{q}) + V_m(q,\dot{q}) \bigtriangledown \varphi(q) - G(q) \tag{27}$$

where $Y_2(q,\dot{q}) \in \mathbb{R}^{n\times m}$ denotes a measurable regression matrix, $\theta \in \mathbb{R}^m$ was introduced in (6), and the auxiliary signal $f(q,\dot{q}) \in \mathbb{R}^n$ is defined as

$$\begin{array}{rcl} f(q,\dot{q}) & \triangleq & \frac{d}{dt}\left(\bigtriangledown\varphi(q)\right) \\ & = & H(q)\dot{q} \end{array} \tag{28}$$

where the Hessian matrix $H(q) \in \mathbb{R}^{n \times n}$ is defined as follows

$$H(q) \triangleq \begin{bmatrix} \frac{\partial^2 \varphi}{\partial q_1^2} & \frac{\partial^2 \varphi}{\partial q_1 \partial q_2} & \cdots & \frac{\partial^2 \varphi}{\partial q_1 \partial q_n} \\ \frac{\partial^2 \varphi}{\partial q_2 \partial q_1} & \frac{\partial^2 \varphi}{\partial q_2^2} & \cdots & \frac{\partial^2 \varphi}{\partial q_2 \partial q_n} \\ \cdots & \cdots & \cdots & \cdots \\ \frac{\partial^2 \varphi}{\partial q_n \partial q_1} & \cdots & \cdots & \frac{\partial^2 \varphi}{\partial q_n^2} \end{bmatrix}.$$

Based on (26) and the subsequent stability analysis, the following adaptive controller introduced in [28] can be utilized

$$\tau \triangleq -k\eta_2 - Y_2(q, \dot{q})\hat{\theta}_2 \tag{29}$$

where $k \in \mathbb{R}$ is a positive constant gain, and $\hat{\theta}_2(t) \in \mathbb{R}^p$ denotes a parameter update law that is generated from the following expression

$$\dot{\hat{\theta}}_2\ (t) \triangleq \Gamma_2 Y_2^T(q, \dot{q})\eta_2 \tag{30}$$

where $\Gamma_2 \in \mathbb{R}^{m \times m}$ is a positive definite, diagonal gain matrix. Note that the trajectory planning is incorporated in the controller through the gradient terms included in (27) and (28). After substituting (29) into (26) the following closed loop error systems can be obtained

$$M\dot{\eta}_2 = -V_m(q, \dot{q})\eta_2 - k\eta_2 + Y_2(q, \dot{q})\tilde{\theta}_2 \tag{31}$$

where $\tilde{\theta}_2(t) \in \mathbb{R}^p$ is defined as follows

$$\tilde{\theta}_2(t) \triangleq \theta - \hat{\theta}_2. \tag{32}$$

4.3 Stability Analysis

Theorem 3 *The adaptive controller given in (29) and (30) ensures that the robot manipulator tracks an obstacle free path to the unique goal configuration in sense that*

$$q(t) \to q^* \ \textit{as}\ t \to \infty$$

provided the control gain k introduced in (29) is selected sufficiently large.

Proof: Let $V_2(q, \eta_2, \tilde{\theta}_2) \in \mathbb{R}$ denote the following nonnegative function

$$V_2 \triangleq \varphi(q) + \gamma \left[\frac{1}{2}\eta_2^T M \eta_2 + \tilde{\theta}_2^T \Gamma_2^{-1} \tilde{\theta}_2 \right]. \tag{33}$$

where $\gamma \in \mathbb{R}$ is an adjustable, positive constant. After taking the time derivative of (33) the following expression can be obtained

$$\dot{V}_2 = \left[\bigtriangledown \varphi(q)\right]^T \dot{q} + \gamma \eta_2^T \left(-k\eta_2 + Y_2(q, \dot{q})\tilde{\theta}_2 \right) - \gamma \tilde{\theta}_2^T \Gamma_2^{-1}\ \dot{\hat{\theta}}_2$$

where (5), (25), (31), and (32) were utilized. By utilizing (24), (30), the following expression can be obtained

$$\dot{V}_2 = - \left\| \bigtriangledown \varphi(q) \right\|^2 - \gamma k \left\| \eta_2 \right\|^2 + \left[\bigtriangledown \varphi(q) \right]^T \eta_2.$$

The expression above can be further simplified as follows

$$\dot{V}_2 \leq -\frac{1}{2} \left\| \bigtriangledown \varphi(q) \right\|^2 - (\gamma k - 2) \left\| \eta_2 \right\|^2 \tag{34}$$

where the following upper bound was utilized

$$\left[\bigtriangledown \varphi(q) \right]^T \eta_2 \leq \frac{1}{2} \left\| \bigtriangledown \varphi(q) \right\|^2 + 2 \left\| \eta_2 \right\|^2.$$

Provided k is selected sufficiently large to satisfy

$$k > \frac{2}{\gamma}, \tag{35}$$

it is clear from (4), (33), and (34) that

$$0 \leq \varphi(q(t)) + \gamma \zeta(q,t) \leq \varphi(q(0)) + \gamma \zeta(q(0),0) \tag{36}$$

where $\zeta(q,t) \in \mathbb{R}$ is defined as

$$\zeta(q,t) \triangleq \left[\frac{m_2(q)}{2} \left\| \eta_2(t) \right\|^2 + \lambda_{\max}\{\Gamma_2^{-1}\} \left\| \tilde{\theta}_2(t) \right\|^2 \right]. \tag{37}$$

From (32), (36), and (37) it is clear that $\eta_2(t)$, $\varphi(q)$, $\tilde{\theta}_2(t)$, $\hat{\theta}_2(t) \in \mathcal{L}_\infty$. Let the region $\mathcal{D}_0$ be defined as follows

$$\mathcal{D}_0 \triangleq \left\{ q(t) \middle| \, 0 \leq \varphi(q(t)) \leq \varphi(q(0)) + \gamma \zeta(q(0),0) \right\}. \tag{38}$$

Hence; (33), (34) and (36) can be utilized to show that $q(t) \in \mathcal{D}_0$ provided $q(0) \in \mathcal{D}_0$ (i.e., $q(t) \in \mathcal{D}_0$ $\forall q(0) \in \mathcal{D}_0$). Based on property P1 given above, we now know that $\bigtriangledown \varphi(q) \in \mathcal{L}_\infty$ $\forall q(0) \in \mathcal{D}_0$. Since $\eta_2(t), \bigtriangledown \varphi(q) \in \mathcal{L}_\infty$ $\forall q(0) \in \mathcal{D}_0$, (24) can be used to conclude that $\dot{q}(t) \in \mathcal{L}_\infty$ $\forall q(0) \in \mathcal{D}_0$; hence, property P1) and (28) can be used to conclude that $f(q,\dot{q}) \in \mathcal{L}_\infty$ $\forall q(0) \in \mathcal{D}_0$. Based on the fact that $M(q)$, $V_m(q,\dot{q})$, $G(q) \in \mathcal{L}_\infty$ $\forall q(0) \in \mathcal{D}_0$ along with the facts that $\bigtriangledown \varphi(q)$, $f(q,\dot{q}) \in \mathcal{L}_\infty$ $\forall q(0) \in \mathcal{D}_0$ can be used along with (27) to prove that $Y_2(q,\dot{q}) \in \mathcal{L}_\infty$ $\forall q(0) \in \mathcal{D}_0$. Based on the facts that $\eta_2(t)$, $Y_2(q,\dot{q})$, $\hat{\theta}_2(t) \in \mathcal{L}_\infty$ $\forall q(0) \in \mathcal{D}_0$ can be used along with (29) to prove that $\tau(t) \in \mathcal{L}_\infty$ $\forall q(0) \in \mathcal{D}_0$. Based on the previous boundedness statements, (31) can be used to show that $\dot{\eta}_2(t) \in \mathcal{L}_\infty \forall q(0) \in \mathcal{D}_0$, and hence, $\bigtriangledown \varphi(q)$, $\eta_2(t)$ are uniformly continuous $\forall q(0) \in \mathcal{D}_0$. From (34), it can also be determined that $\bigtriangledown \varphi(q)$, $\eta_2(t) \in \mathcal{L}_2$ $\forall q(0) \in \mathcal{D}_0$. From these facts, Barbalat's Lemma [28] can be used to show that $\bigtriangledown \varphi(q)$, $\eta_2(t) \to 0$ as $t \to \infty$ $\forall q(0) \in \mathcal{D}_0$. Since $\bigtriangledown \varphi(q) \to 0$, property P4) given above can be used to prove that $q(t) \to q^*$ as $t \to \infty$ $\forall q(0) \in \mathcal{D}_0$. To ensure that $q(t)$ will remain in a collision-free region, we must account for the effects of the $\gamma \zeta(q(0),0)$ term introduced in the definition of the region $\mathcal{D}_0$ given in (38). To this end, we first define the region $\mathcal{D}_1$ as follows

$$\mathcal{D}_1 \triangleq \left\{ q(t) \middle| \, 0 \leq \varphi(q(t)) < 1 \right\} \tag{39}$$

where $\mathcal{D}_1$ denotes the largest collision-free region, which is based on the definition of the function $\varphi(q) : \mathcal{D} \rightarrow [0, 1]$. It is now clear from (38) and (39) that if the weighting constant γ is selected sufficiently small to satisfy

$$\varphi(q(0)) + \gamma\zeta(q(0), 0) < 1, \tag{40}$$

hence making the upper bound of $\mathcal{D}_1$ greater than the upper bound of $\mathcal{D}_0$, then $\mathcal{D}_0 \subset \mathcal{D}_1$, and hence, the robot manipulator tracks an obstacle free path. ■

5 Experimental Verification

Experimental results were obtained by implementing the adaptive VFC and the navigation function controller on a Barrett Whole Arm Manipulator (WAM). The experimental testbed and results from implementing the controllers are provided in the following sections.

5.1 Experimental Setup

The WAM testbed depicted in Fig. 1 was utilized to implement the VFC and the navigation function controller. For simplicity, 5 links of the robot were locked at a fixed, specified angle during the experiment, and the remaining links of the manipulator were used to enable the manipulator to move along a planar trajectory. Specifically, a joint-space proportional derivative (PD) controller was utilized to servo the WMR to the following initial joint configuration for the adaptive VFC experiment (in [deg])

$$q(0) = \begin{bmatrix} 0 & 90 & -90 & 60 & 90 & 20 & 0 \end{bmatrix}^T$$

and to the following joint configuration for the navigation function experiment (in [deg])

$$q(0) = \begin{bmatrix} -58.84 & 90 & 90 & 140.72 & 11.5 & 84.5 & 0 \end{bmatrix}^T.$$

Once the WAM was servoed to the initial joint configuration, links 2, 3, 5, 6 and 7 were locked, resulting in a planar configuration with links 1 and 4 (see Fig. 1). The resulting forward kinematics and manipulator Jacobian for the planar-WAM are given as follows

$$\begin{bmatrix} x_1 \\ x_2 \end{bmatrix} = \begin{bmatrix} \ell_1 \cos(q_1) + \ell_4 \cos(q_1 + q_4) \\ \ell_1 \sin(q_1) + \ell_4 \sin(q_1 + q_4) \end{bmatrix}$$

$$J(q) = \begin{bmatrix} -\ell_1 \sin(q_1) - \ell_4 \sin(q_1 + q_4) & -\ell_4 \sin(q_1 + q_4) \\ \ell_1 \cos(q_1) + \ell_4 \cos(q_1 + q_4) & \ell_4 \cos(q_1 + q_4) \end{bmatrix} \tag{41}$$

where $\ell_1 = 0.558$ [m] and $\ell_4 = 0.291$ [m]. The dynamics of the planar-WAM can be expressed in the following form [29]

$$\begin{aligned} \tau = & \begin{bmatrix} M_{11} & M_{12} \\ M_{21} & M_{22} \end{bmatrix} \begin{bmatrix} \ddot{q}_1 \\ \ddot{q}_4 \end{bmatrix} + \begin{bmatrix} V_{m_{11}} & V_{m_{12}} \\ V_{m_{21}} & V_{m_{22}} \end{bmatrix} \begin{bmatrix} \dot{q}_1 \\ \dot{q}_4 \end{bmatrix} \\ & + \begin{bmatrix} f_{d_1} & 0 \\ 0 & f_{d_4} \end{bmatrix} \begin{bmatrix} \dot{q}_1 \\ \dot{q}_4 \end{bmatrix}. \end{aligned} \tag{42}$$

In (42), the elements of the inertia and centripetal-Coriolis matrices are given as

$$
\begin{aligned}
M_{11} &= p_1 + 2p_2 cos(q_4) \\
M_{12} &= p_3 + p_2 cos(q_4) \\
M_{21} &= p_3 + p_2 cos(q_4) \\
M_{22} &= p_3
\end{aligned}
$$

$$
\begin{aligned}
V_{m_{11}} &= -p_2 sin(q_4)\dot{q}_4 \\
V_{m_{12}} &= -p_2 sin(q_4)\dot{q}_1 - p_2 sin(q_4)\dot{q}_4 \\
V_{m_{21}} &= p_2 sin(q_4)\dot{q}_1 \\
V_{m_{22}} &= 0
\end{aligned}
$$

where p_1, p_2, p_3 denote unknown constant inertial parameters, and $f_{d_1} = 6.8$ [Nm·s] and $f_{d_4} = 3.8$ [Nm·s]. The gravitational effects are not included in (42) due to the plane of motion of the manipulator.

The links of the WAM manipulator are driven by brushless motors supplied with sinusoidal electronic commutation. Each axis has encoders located at the motor shaft for link position measurements. Since no tachometers are present for velocity measurements, link velocity signals are calculated via a filtered backwards difference algorithm. An AMD Athlon 1.2GHz PC operating QNX 6.2.1 RTP (Real Time Platform), a real-time micro-kernel based operating system, hosts the control, detection and identification algorithms which were written in "C++". Qmotor 3.0 [24], was used to facilitate real time graphing, data logging and on-line gain adjustment. Data acquisition and control implementation were performed at a frequency of 1.0 [kHz] using the ServoToGo I/O board.

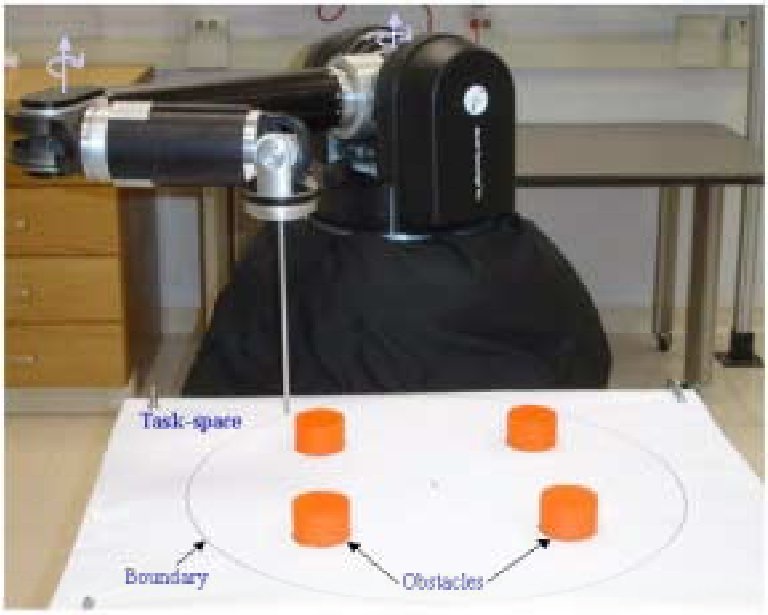

Figure 1: Front view of the experimental setup

5.2 Experimental Results

5.2.1 Adaptive VFC Experiment

The following task-space velocity field for a planar, circular contour was utilized for the experiment [4]

$$\vartheta(x) = -2K(x)f(x)\begin{bmatrix} (x_1 - x_{c1}) \\ (x_2 - x_{c2}) \end{bmatrix} + 2c(x)\begin{bmatrix} -(x_2 - x_{c2}) \\ (x_1 - x_{c1}) \end{bmatrix} \tag{43}$$

where $x_{c1} = 0.54$ [m] and $x_{c2} = 0.04$ [m] denote the circle center, and the functions $f(x)$, $K(x)$, and $c(x) \in \mathbb{R}$ are defined as follows [4]

$$\begin{aligned} f(x) &= (x_1 - x_{c1})^2 + (x_2 - x_{c2})^2 - r_o^2 \\ K(x) &= \frac{k_0^*}{\sqrt{f^2(x)}\left\|\frac{\partial f(x)}{\partial x}\right\| + \epsilon} \\ c(x) &= \frac{c_0 \exp\left(-\mu\sqrt{f^2(x)}\right)}{\left\|\frac{\partial f(x)}{\partial x}\right\|}. \end{aligned} \tag{44}$$

In (44), $r_o = 0.2$ [m] denotes the circle diameter, and the parameters $\epsilon = 0.005$ [m^3], $\mu = 20$ [m^{-1}], $k_0^* = 0.25$ [ms^{-1}], and $c_0 = 0.25$ [ms^{-1}] were selected according to [4]. The task-space velocity field is depicted in Fig. 2. The development in Appendix A indicates that the velocity field in (43) satisfies the condition given in (2). To implement the adaptive VFC given in (11) and (12), the task-space velocity field is transformed into a joint-space velocity field as follows $\vartheta(q) = J^{-1}(q)\vartheta(x)$.

The following values were recorded as follows

$$K = diag(25, 15) \qquad \Gamma = diag(3, 1, 5)$$

where $diag(\cdot)$ denotes a diagonal matrix with the arguments as the diagonal entries, the resulting velocity field tracking errors are given in Fig. 2. Fig. 4 depicts the parameter estimates, and Fig. 5 depicts the control torque inputs.

5.2.2 Adaptive Navigation Function Control Experiment

For the navigation function control experiment, four circular obstacles with known dimensions were placed in known locations in the task-space (see Fig. 1). The actual size of the obstacles and task-space is then modified in the algorithm to accommodate for the term $\gamma\zeta(q(0), 0)$ given in (36) and (37) (i.e., the configuration-space was reduced to ensure obstacle avoidance). To modify the configuration-space according to (36) and (37), exact knowledge of the inertial parameters is required. Since these parameters are unknown, an upper bound for $\zeta(q(0), 0)$ was utilized based on known upper bounds for the inertial parameters. The modifications to the configuration-space are depicted in Figure 6. A task-space navigation function was developed to encapsulate the obstacles and the task-space boundary as follows

$$\varphi(x) = \frac{\|x - x^*\|^2}{\left(\|x - x^*\|^{28} + \beta_0\beta_1\beta_2\beta_3\beta_4\right)^{1/14}} \tag{45}$$

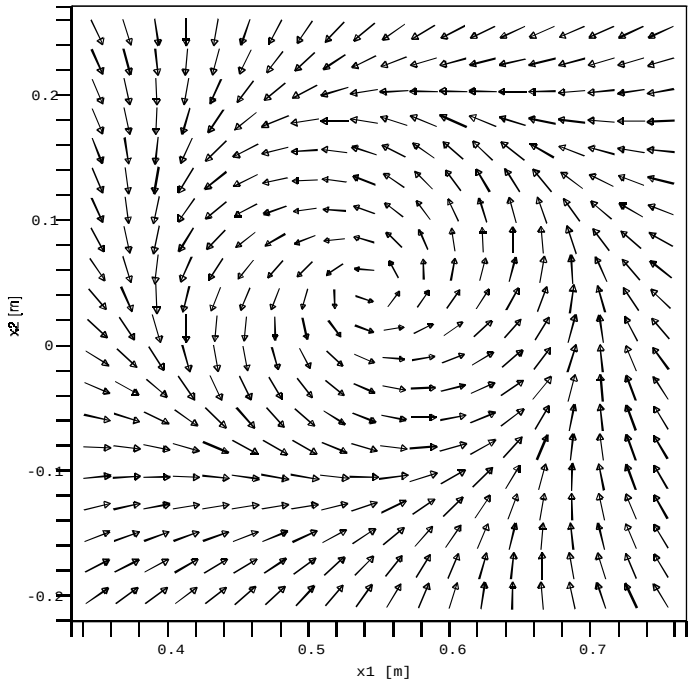

Figure 2: Desired Trajectory

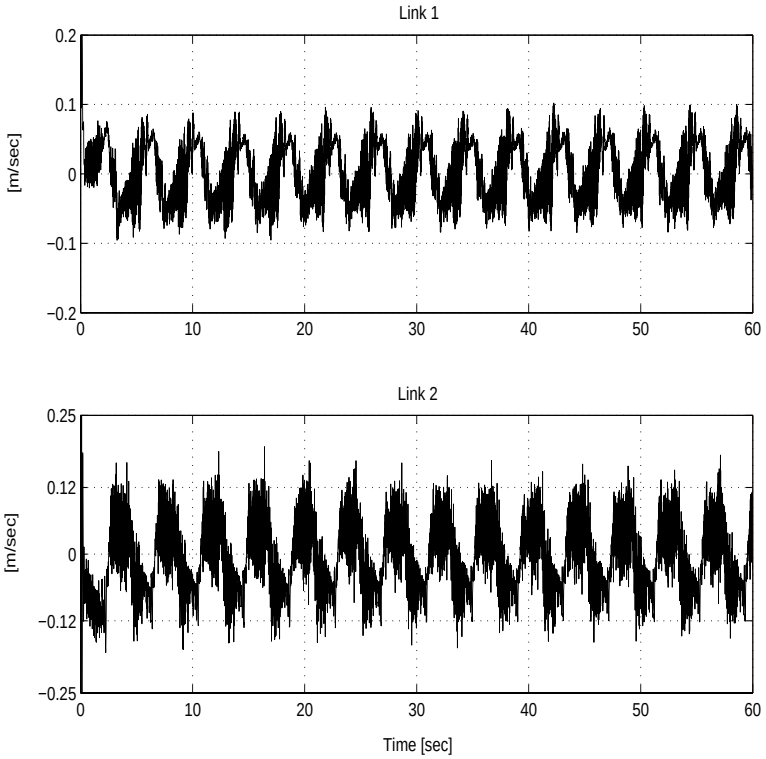

Figure 3: Velocity field tracking errors.

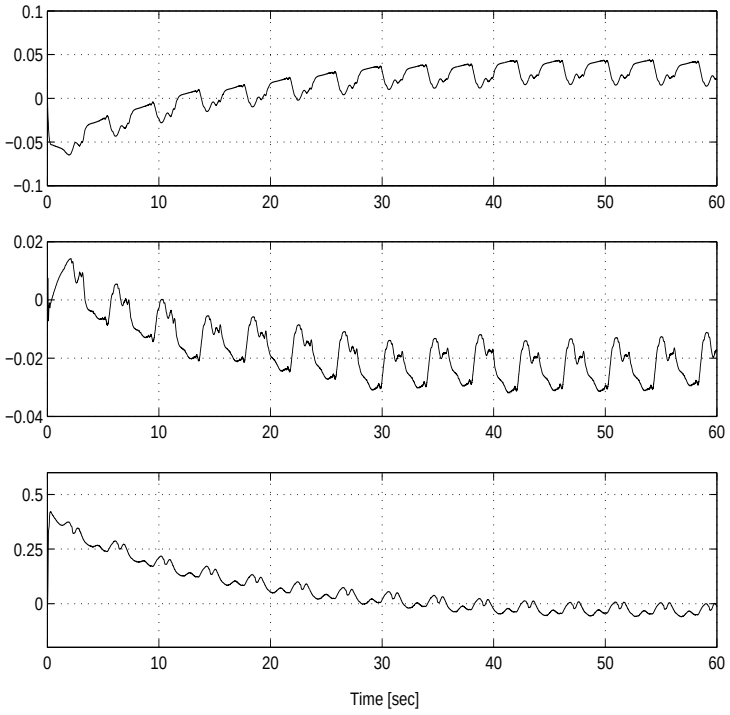

Figure 4: Parameter estimates.

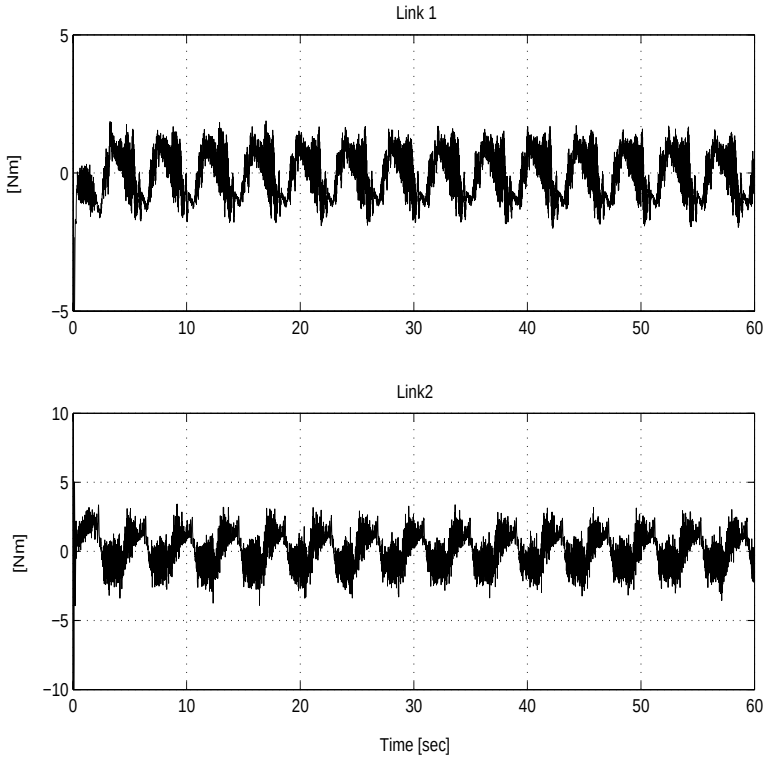

Figure 5: Control torque inputs.

where $x(t) \triangleq [x_1(t),\, x_2(t)]^T \in \mathbb{R}^2$ denote the actual task-space position of the WAM end-effector, $x^* \triangleq [x_1^*,\, x_2^*]^T \in \mathbb{R}^2$ denotes the task-space goal position. In (45), the boundary function $\beta_0(x) \in \mathbb{R}$ and the obstacle functions $\beta_1(x)$, $\beta_2(x)$, $\beta_3(x)$, $\beta_4(x) \in \mathbb{R}$ are defined as follows

$$\begin{aligned} \beta_0 &= r_0^2 - (x_1 - x_{1r_0})^2 - (x_2 - x_{2r_0})^2 \\ \beta_1 &= (x_1 - x_{r_1})^2 + (x_2 - x_{2r_1})^2 - r_1^2 \\ \beta_2 &= (x_1 - x_{r_2})^2 + (x_2 - x_{2r_2})^2 - r_2^2 \\ \beta_3 &= (x_1 - x_{r_3})^2 + (x_2 - x_{2r_3})^2 - r_3^2 \\ \beta_4 &= (x_1 - x_{r_4})^2 + (x_2 - x_{2r_4})^2 - r_4^2. \end{aligned} \tag{46}$$

In (46), $(x_1 - x_{1r_i})$ and $(x_2 - x_{2r_i})$ where $i = 0, 1, 2, 3, 4$ are the respective centers of the boundary and obstacles, and r_0, r_1, r_2, r_3, $r_4 \in \mathbb{R}$ are the respective radii of the boundary and obstacles. From (45) and (46) it is clear that the model-space is a circle that excludes four smaller circles described by the obstacle functions $\beta_1(x)$, $\beta_2(x)$, $\beta_3(x)$, $\beta_4(x)$. Based on the known location and size of the obstacles and task-space boundary, the model-space configuration parameters were selected as follows (in [m])

$$\begin{array}{lll} x_{1r_0} = 0.5064 & x_{2r_0} = -0.0275 & r_0 = 0.28 \\ x_{1r_1} = 0.63703 & x_{2r_1} = 0.11342 & r_1 = 0.03 \\ x_{1r_2} = 0.4011 & x_{2r_2} = 0.0735 & r_2 = 0.03 \\ x_{1r_3} = 0.3788 & x_{2r_3} = -0.1529 & r_3 = 0.03 \\ x_{1r_4} = 0.6336 & x_{2r_4} = -0.12689 & r_4 = 0.03. \end{array}$$

To implement the navigation function based controller given in (29) and (30) the joint-space dynamic model given in (42) was transformed to the task-space as follows [6]

$$\tau^* = M^*(x)\ddot{x} + V_m^*(x, \dot{x})\dot{x} + F_d^*\dot{x}$$

where

$$\begin{aligned} \tau^* &= J^{-T}\tau, \quad M^* = J^{-T} \begin{bmatrix} M_{11} & M_{12} \\ M_{21} & M_{22} \end{bmatrix} J^{-1} \\ V_m^* &= J^{-T} \left(\begin{bmatrix} V_{m_{11}} & V_{m_{12}} \\ V_{m_{21}} & V_{m_{22}} \end{bmatrix} - \begin{bmatrix} M_{11} & M_{12} \\ M_{21} & M_{22} \end{bmatrix} J^{-1}\dot{J} \right) J^{-1} \\ F_d^* &= J^{-T} \begin{bmatrix} f_{d_1} & 0 \\ 0 & f_{d_4} \end{bmatrix} J^{-1} \end{aligned}$$

where $J^{-1}(q)$ can be determined from (41) as follows

$$J^{-1}(q) = \begin{bmatrix} \dfrac{\cos(q_1 + q_4)}{\ell_1 \sin q_4} & \dfrac{\sin(q_1 + q_4)}{\ell_1 \sin q_4} \\ -\dfrac{\ell_1 \cos q_1 + \ell_4 \cos(q_1 + q_4)}{\ell_1 \ell_4 \sin q_4} & -\dfrac{\ell_1 \sin q_1 + \ell_4 \sin(q_1 + q_4)}{\ell_1 \ell_4 \sin q_4} \end{bmatrix}.$$

After adjusting the control gains to ensure the gain conditions (35) and (40) are satisfied, the following values were recorded

$$k = 45 \qquad \Gamma_2 = diag\,(0.02, 0.01, 0.01)\,,$$

the resulting actual trajectory of the WAM end-effector is provided in Fig. 6. Fig. 6 illustrates that the WAM end-effector avoids the actual obstacles as it moves to the goal point. The parameter estimates and control torque inputs are provided in Figs. 7 and 8, respectively.

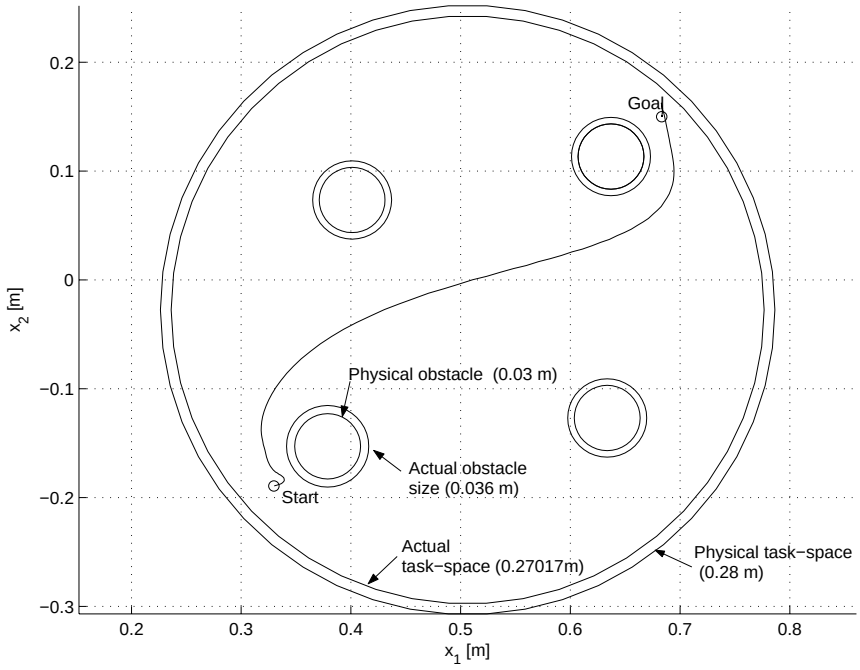

Figure 6: Actual trajectory of the WAM robot.

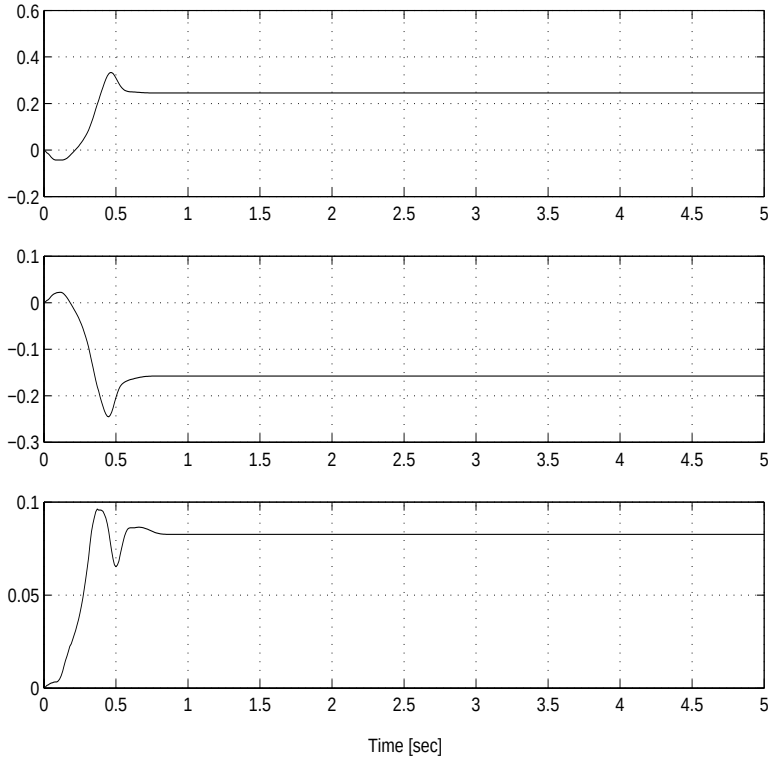

Figure 7: Parameter estimates.

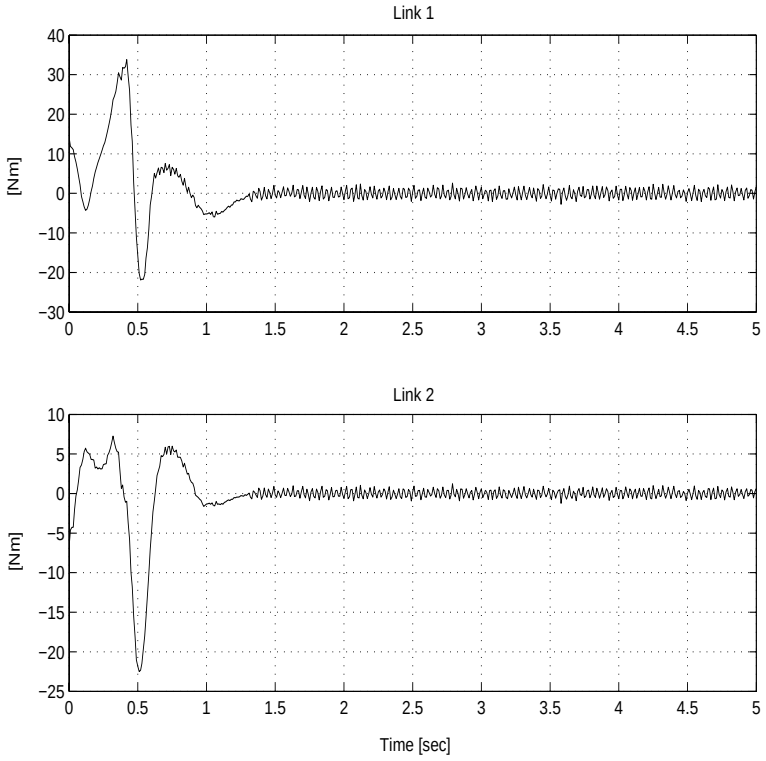

Figure 8: Control torque inputs.

Remark 5 *The adaptive control results achieved in Sections 3.3 and 4.3 proves that* $\dot{\hat{\theta}}_1(t)$ *and* $\dot{\hat{\theta}}_2(t) \to 0$ *as* $t \to \infty$, *therefore the parameter estimates* $\theta(t)$ *are not identified. The values of the estimates that are reached could be different from one experimental run to another. The parameter estimates may not become constant due to steady-state tracking errors.*

6 Conclusion

Two trajectory planning and adaptive tracking controllers are presented. The benchmark adaptive tracking controller by Slotine [28] was modified to achieve velocity field tracking in the presence of parametric uncertainty in the robot dynamics. By incorporating a norm squared gradient term to the VFC, the boundedness of all signals can be proven without the typical assumption that bounds the integral of the velocity field. An extension was then provided that also modifies a standard adaptive controller by incorporating a gradient based term. Using standard backstepping techniques, a Lyapunov analysis was used to prove that a navigation function could be incorporated in the control design to ensure the robot remained on an obstacle free path within an expanded configuration space to reach a goal configuration. Experimentation results illustrated proof of validation of the adaptive VFC and navigation function tracking controllers.

References

[1] J. Barraquand and J. C. Latombe, "A Monte-Carlo Algorithm for Path Planning with Many

Degrees of Freedom," *Proc. of the IEEE Int. Conf. on Robotics and Automation*, Cincinnati, Ohio, 1990, pp. 584-589.

[2] J. Barraquand, B. Langlois, and J. C. Latombe, "Numerical Potential Fields Techniques for Robot Path Planning," *IEEE Trans. on Systems, Man, and Cybernetics*, Vol. 22, pp. 224-241, (1992).

[3] A. Bemporad, A. De Luca, and G. Oriolo, "Local Incremental Planning for a Car-Like Robot Navigating Among Obstacles," *Proc. of the IEEE Int. Conf. on Robotics and Automation*, Minneapolis, Minnesota, 1996, pp. 1205-1211.

[4] I. Cervantes, R. Kelly, J. Alvarez-Ramirez, and J. Moreno, "A Robust Velocity Field Control," *IEEE Trans. on Control Systems Technology*, Vol. 10, No. 6, pp. 888-894, (2002).

[5] C. I. Connolly, J. B. Burns, and R. Weiss, "Path Planning Using Laplace's Equation," *Proc. of the IEEE Int. Conf. on Robotics and Automation*, Cincinnati, Ohio, 1990, pp. 2102-2106.

[6] W. E. Dixon, A. Behal, D. M. Dawson, and S. Nagarkatti, *Nonlinear Control of Engineering Systems: A Lyapunov-Based Approach*, Birkhäuser Boston, 2003.

[7] S. S. Ge and Y. J. Cui, "New Potential Functions for Mobile Robot Path Planning," *IEEE Trans. on Robotics and Automation*, Vol. 16, No. 5, pp. 615-620, (2000).

[8] J. Guldner and V. I. Utkin, "Sliding Mode Control for Gradient Tracking and Robot Navigation Using Artificial Potential Fields," *IEEE Trans. on Robotics and Automation*, Vol. 11, No. 2, pp. 247-254, (1995).

[9] J. Guldner, V. I. Utkin, H. Hashimoto, and F. Harashima, "Tracking Gradients of Artificial Potential Field with Non-Holonomic Mobile Robots," *Proc. of the American Control Conf.*, Seattle, Washington, 1995, pp. 2803-2804.

[10] H. K. Khalil, *Nonlinear Systems*, Third edition, Prentice Hall, 2002.

[11] O. Khatib, *Commande dynamique dans l'espace opérational des robots manipulateurs en présence d'obstacles*, Ph.D. Dissertation, École Nationale Supéieure de l'Aeéronatique et de l'Espace (ENSAE), France, 1980.

[12] O. Khatib, "Real-Time Obstacle Avoidance for Manipulators and Mobile Robots," *Inter. Journal of Robotics Research*, Vol. 5, No. 1, pp. 90-99, (1986).

[13] D. E. Koditschek, "Exact Robot Navigation by Means of Potential Functions: Some Topological Considerations," *Proc. of the IEEE Int. Conf. on Robotics and Automation*, Raleigh, North Carolina, 1987, pp. 1-6.

[14] D. E. Koditschek and E. Rimon, "Robot Navigation Functions on Manifolds with Boundary," *Adv. Appl. Math.*, Vol. 11, pp. 412-442, (1990).

[15] K. J. Kyriakopoulos, H. G. Tanner, and N. J. Krikelis, "Navigation of Nonholonomic Vehicles in Complex Environments with Potential Fields and Tracking," *Int. J. Intell. Contr. Syst.*, Vol. 1, No. 4, pp. 487-495, (1996).

[16] J. C. Latombe, *Robot Motion Planning*, Kluwer Academic Publishers: Boston, Massachusetts, 1991.

[17] J. P. Laumond, P. E. Jacobs, M. Taix, and R. M. Murray, "A Motion Planner for Nonholonomic Mobile Robots," *IEEE Trans. on Robotics and Automation*, Vol. 10, No. 5, pp. 577-593, (1994).

[18] D. Lee and P. Li, "Passive Bilateral Feedforward Control of Linear Dynamically Similar Teleoperated Manipulators," *IEEE Trans. on Robotics and Automation*, Vol. 19, No. 3, pp. 443-456 (2003).

[19] F. Lewis, C. Abdallah, and D. Dawson, *Control of Robot Manipulators*, New York: MacMillan Publishing Co., 1993.

[20] J. Li and P. Li, "Passive Velocity Field Control (PVFC) Approach to Robot Force Control and Contour Following," *Proc. of the Japan/USA Symposium on Flexible Automation*, Ann Arbor, Michigan, 2000.

[21] P. Li, "Adaptive Passive Velocity Field Control," *Proc. of the American Controls Conference*, San Diego, California, 1999, pp. 774-779.

[22] P. Li and R. Horowitz, "Passive Velocity Field Control of Mechanical Manipulators," *IEEE Trans. on Robotics and Automation*, Vol. 15, No. 4, pp. 751-763, (1999).

[23] P. Li and R. Horowitz, "Passive Velocity Field Control (PVFC): Part II - Application to Contour Following," *IEEE Trans. on Automatic Control*, Vol. 46, No. 9, pp. 1360-1371, (2001).

[24] M. Loffler, N. Costescu, and D. Dawson, "QMotor 3.0 and the QMotor Robotic Toolkit - An Advanced PC-Based Real-Time Control Platform", *IEEE Control Systems Magazine*, Vol. 22, No. 3, pp. 12-26 June, 2002.

[25] A. De Luca and G. Oriolo, "Local Incremental Planning for Nonholonomic Mobile Robots," *Proc. of the IEEE Int. Conf. on Robotics and Automation*, San Diego, California, 1994, pp. 104-110.

[26] Z. Qu, *Robust Control of Nonlinear Uncertain Systems*, New York: John Wiley & Sons, 1998.

[27] E. Rimon and D. E. Koditschek, "Exact Robot Navigation Using Artificial Potential Function," *IEEE Trans. on Robotics and Automation*, Vol. 8, No. 5, pp. 501-518, (1992).

[28] J.J.E. Slotine and W. Li, *Applied Nonlinear Control*, Englewood Cliff, NJ: Prentice Hall, Inc., 1991.

[29] M. W. Spong and M. Vidyasagar, *Robot Dynamics and Control*, New York: John Wiley and Sons, Inc., 1989.

[30] H. G. Tanner and K. J. Kyriakopoulos, "Nonholonomic Motion Planning for Mobile Manipulators," *Proc. of the IEEE Int. Conf. on Robotics and Automation*, San Francisco, California, 2000, pp. 1233-1238.

[31] H. G. Tanner, S. G. Loizou, and K. J. Kyriakopoulos, "Nonholonomic Navigation and Control of Cooperating Mobile Manipulators," *IEEE Trans. on Robotics and Automation*, Vol. 19, No. 1, pp. 53-64, (2003).

[32] R. Volpe and P. Khosla, "Artificial Potential with Elliptical Isopotential Contours for Obstacle Avoidance," *Proc. of the IEEE Conf. on Decision and Control*, Los Angeles, California, 1987, pp. 180-185.

[33] M. Yamakita, T. Yazawa, X.-Z. Zheng, and K. Ito, "An Application of Passive Velocity Field Control to Cooperative Multiple 3-Wheeled Mobile Robots," *Proceedings of the IEEE/RJS Int. Conf. on Intelligent Robots and Systems*, Victoria, B. C., Canada, 1998, pp. 368-373.

[34] M. Yamakita, K. Suzuki, X.-Z. Zheng, M. Katayama, and K. Ito, "An Extension of Passive Velocity Field Control to Cooperative Multiple Manipulator Systems," *Proc. of the IEEE/RJS Int. Conf. on Intelligent Robots and Systems*, Grenoble, France, 1997, pp. 11-16.

A Experimental Velocity Field Selection

This VFC development is based on the selection of a velocity field that is first order differentiable, and that a first order differentiable, nonnegative function $V(q) \in \mathbb{R}$ exists such that the following inequality holds

$$\frac{\partial V(x)}{\partial x}\vartheta(x) \leq -\gamma_3(\|x\|) + \zeta_0 \tag{47}$$

where $\frac{\partial V(q)}{\partial q}$ denotes the partial derivative of $V(q)$ with respect to $q(t)$, $\gamma_3(\cdot) \in \mathbb{R}$ is a class $\mathcal{K}$ function[3], and $\zeta_0 \in \mathbb{R}$ is a nonnegative constant. To prove that the velocity field in (43) and (44) satisfies the condition in (47), let $V(x) \in \mathbb{R}$ denote the following nonnegative, continuous differentiable function

$$V(x) \triangleq \frac{1}{2}x^T x. \tag{48}$$

After taking the time derivative of (48) and substituting (43) for $\dot{x}(t)$, the following inequality can be developed

$$\dot{V} = x^T\vartheta(x) \leq -\gamma_3(x) + \zeta_0 \tag{49}$$

where $\gamma_3(x)$ and ζ_0 were defined in (47).

To prove the inequality given in (49) we must find $\gamma_3(x)$ and ζ_0. To this end, we rewrite $x^T\vartheta(x)$ as follows

$$x^T\vartheta(x) = -2K(x)f(x)x^T x \tag{50}$$

where (43) has been utilized, and x_{c1} and x_{c2} of (43) and (44) are set to zero for simplicity and without loss of generality. By substituting (44) into (50) for $K(x)$ and $f(x)$, the following expression can be obtained

$$x^T\vartheta(x) = \frac{-k_0^* \|x\|^4 + k_0^* r_o^2 \|x\|^2}{\left|\left(\|x\|^2 - r_o^2\right)\right| \|x\| + \frac{\epsilon}{2}}. \tag{51}$$

After utilizing the following inequality

$$\|x\|^2 \leq \delta \|x\|^4 + \frac{1}{\delta}$$

[3] A continuous function $\alpha : [0, \alpha) \to [0, \infty)$ is said to belong to class $\mathcal{K}$ if it is strictly increasing and $\alpha(0) = 0$ [10].

where $\delta \in \mathbb{R}$ is a positive constant, the inequality given in (49) can be determined from (51) where

$$\gamma_3(x) = \frac{k_0^* \left(1 - r_o^2 \delta\right) \|x\|^4}{\left(\|x\|^2 + r_o^2\right) \|x\| + \frac{\epsilon}{2}}$$

and

$$\zeta_0 = \frac{2k_0^* r_o^2}{\delta \epsilon}.$$

Provided δ is selected according to the following inequality

$$\delta < \frac{1}{r_o^2},$$

then $\gamma_3(x)$ can be shown to be a class $\mathcal{K}$ function.

B Lemma 1

Given a continuously differentiable function, denoted by $V(q)$, that satisfies the following inequalities

$$0 < \gamma_1(\|q\|) \leq V(q) \leq \gamma_2(\|q\|) + \xi_b \tag{52}$$

with a time derivative that satisfies the following inequality

$$\dot{V}(q) \leq -\gamma_3(\|q\|) + \xi_0, \tag{53}$$

then $q(t)$ is GUB, where $\gamma_1(\cdot)$, $\gamma_2(\cdot)$, $\gamma_3(\cdot)$ are class $\mathcal{K}$ functions, and ξ_0, $\xi_b \in \mathbb{R}$ denote positive constants.

Proof:[4] Let $\Omega \in \mathbb{R}$ be a positive function defined as follows

$$\Omega \triangleq \gamma_3^{-1}(\xi_0) > 0 \tag{54}$$

where $\gamma_3^{-1}(\cdot)$ denotes the inverse of $\gamma_3(\cdot)$, and let $B(0, \Omega)$ denote a ball centered about the origin with a radius of Ω. Consider the following 2 possible cases.

The initial condition $q(t_0)$ lies outside the ball $B(0, \Omega)$ as follows

$$\Omega < \|q(t_0)\| \leq \Omega_1 \tag{55}$$

where $\Omega_1 \in \mathbb{R}$ is a positive constant. To facilitate further analysis, we define the operator $d(\cdot)$ as follows

$$d(\Omega_1) \triangleq (\gamma_1^{-1} \circ \gamma_2)(\Omega_1) + \gamma_1^{-1}(\xi_b) > 0 \tag{56}$$

where $(\gamma_1^{-1} \circ \gamma_2)$ denotes the composition of the inverse of $\gamma_1(\cdot)$ with $\gamma_2(\cdot)$ (i.e., the inverse of the function $\gamma_1(\cdot)$ is applied to the function $\gamma_2(\cdot)$). After substituting the constant $d(\Omega_1)$ into $\gamma_1(\cdot)$, the following inequalities can be determined

$$\gamma_1(d(\Omega_1)) = \gamma_2(\Omega_1) + \xi_b \geq \gamma_2(\|q(t_0)\|) + \xi_b \geq V(q(t_0)) \tag{57}$$

[4] This proof is based on the proof for Theorem 2.14 in [26].

where the inequalities provided in (52) and (55) were utilized.

Assume that $q(\tau) \in \mathbb{R}$ for $t_0 \leq \tau \leq t < \infty$ lies outside the ball $B(0, \Omega)$ as follows

$$\Omega < \|q(\tau)\|. \tag{58}$$

From (53) and (58), the following inequality can be determined

$$\dot{V}(q(\tau)) \leq -\gamma_3(\Omega) + \xi_0,$$

and hence, from the definition for Ω in (54), it is clear that

$$\dot{V}(q(\tau)) \leq 0. \tag{59}$$

By utilizing (57) and the result in (59), the following inequalities can be developed for some constant $\Delta\tau$

$$\gamma_1(d(\Omega_1)) \geq V(q(t_0)) \geq V(q(\tau)) \geq V(q(\tau + \Delta\tau)) \geq \gamma_1(\|q(\tau + \Delta\tau)\|). \tag{60}$$

Since $\gamma_1(\cdot)$ is a class $\mathcal{K}$ function, (56) and (60) can be used to develop the following inequality

$$\|q(t)\| \leq d(\Omega_1) = (\gamma_1^{-1} \circ \gamma_2)(\Omega_1) + \gamma_1^{-1}(\xi_b) \qquad \forall t \geq t_0$$

provided the assumption in (58) is satisfied. If the assumption in (58) is not satisfied, then

$$\|q(t)\| \leq \Omega = \gamma_3^{-1}(\xi_0) \qquad \forall t \geq t_0. \tag{61}$$

Hence, $q(t)$ is GUB for Case A.

The initial condition $q(t_0)$ lies inside the ball $B(0, \Omega)$ as follows

$$\|q(t_0)\| \leq \Omega \leq \Omega_1.$$

If $q(t)$ remains in the ball, then the inequality developed in (61) will be satisfied. If $q(t)$ leaves the ball, then the results from Case A can be applied. Hence, $q(t)$ is GUB for Case B. ■